

International Conference on Computational Science, ICCS 2011

Discontinuous Galerkin and Mixed-Hybrid Finite Element Approach to Two-Phase Flow in Heterogeneous Porous Media with Different Capillary Pressures

Radek Fučík and Jiří Mikyška

Faculty of Nuclear Sciences and Physical Engineering, Czech Technical University in Prague, Trojanova 13, 120 00 Prague, Czech Republic

Abstract

A modern numerical scheme for simulation of flow of two immiscible and incompressible phases in inhomogeneous porous media is proposed. The method is based on a combination of the mixed-hybrid finite element (MHFE) and discontinuous Galerkin (DG) methods. The combined approach allows for accurate approximation of the flux at the boundary between neighboring finite elements, especially in heterogeneous media. In order to simulate the non-wetting phase pooling at material interfaces (i.e., the barrier effect), we extend the approach proposed in Hoteit and Firoozabadi (2008) by considering the extended capillary pressure condition. The applicability of the MHFE-DG method is demonstrated on benchmark solutions and simulations of laboratory experiments of two-phase flow in highly heterogeneous porous media.

Keywords: Two-phase flow in porous medium, Capillary barrier, Heterogeneous porous medium, Mixed-hybrid finite element method, Discontinuous Galerkin method

1. Introduction

Understanding and protection of drinking water resources is one of the most important modern missions of the mathematical modeling of flow in the subsurface. Due to industrial activities, the water saturated aquifers are endangered by substances with a very low solubility in water such as oil or chlorinated hydrocarbons. When these substances, generally referred to as Non-Aqueous Phase Liquids (NAPLs), enter the aquifer, they can serve as a long-time source of groundwater contamination. A prediction of their behavior in the subsurface is an important step towards their partial or complete removal from the contaminated area. Therefore, two-phase processes have been studied intensively in engineering, soil physics, and hydrogeology over several decades [1], [2]. The propagation of NAPLs through water saturated zones is usually driven by two primary mechanisms. The NAPL is displaced due to external forces (externally imposed flow, gravity) and capillarity. Especially in heterogeneous porous media, the capillary forces have an important impact on the flow across interfaces between materials with different capillarity properties, [3]. Besides the groundwater protection, two-phase flow models play an important role in the petroleum reservoir engineering and deep CO₂ sequestration [4].

Email address: radek.fucik@jfji.cvut.cz, jiri.mikyska@jfji.cvut.cz (Radek Fučík and Jiří Mikyška)

In order to model two-phase flow in heterogeneous porous materials, a large number of numerical methods have been developed based on the finite difference (FD), finite volume (FV), or finite element (FE) methods. These methods have typically low accuracy. The FD method is applicable only for orthogonal meshes and the conventional FV method is strongly influenced by the mesh quality and orientation, which makes these methods unsuitable for a large number of real world problems modeled using unstructured grids. There have been attempts to improve accuracy of the FV approach on unstructured meshes by using multi-point flux approximation techniques. Another effort to develop a higher-order numerical scheme was based on the mixed-hybrid finite element (MHFE) method such as [5]. However, none of the proposed MHFE formulations were able to simulate two-phase flow in heterogeneous porous media with discontinuities in saturations at material interfaces that are caused by different capillary pressure functions. Recently, Hoteit and Firoozabadi [6], [7], [8], developed a higher-order numerical method that combines the MHFE approach and the discontinuous Galerkin (DG) method, together denoted as MHFE-DG. Their approach can be used to model two-phase flow in a heterogeneous porous medium with sharp jumps in saturation across material interfaces. We build upon their ideas and extend their approach so that the scheme can simulate the non-wetting phase pooling at material heterogeneity. The use of MHFE-DG allows for accurate representation of the phase velocities across sides of finite elements and approximates saturation as piecewise discontinuous per elements. This facilitates discretization of the two-phase flow problems especially in case of heterogeneous porous materials and fractured media, where the saturation is often discontinuous across sharp heterogeneity interfaces.

The paper is organized in the following way. In Section 2, we review the two-phase flow equations and extended capillary pressure condition at heterogeneity interfaces. In Section 3, we reformulate the problem using the flow potentials and specially introduced velocities. In Section 4, we describe derivation of the numerical scheme, resulting system of linear equations, and the computational algorithm. In Section 5, we use benchmark solutions to verify convergence of the numerical scheme in both homogeneous and heterogeneous cases. In Section 6, we present application of the MHFE-DG scheme for simulation of a laboratory experiment of two-phase flow in a highly heterogeneous porous medium.

2. Model Equations

The mathematical model of multi-phase flow in porous media is based on the assumption that every fluid phase is governed by the continuity theorem and the Darcy law. In the following, we consider a wetting phase and a non-wetting phase indexed by w and n , respectively. The α -phase mass balance for $\alpha \in \{w, n\}$ has the following form

$$\frac{\partial(\phi \varrho_\alpha S_\alpha)}{\partial t} + \nabla \cdot (\varrho_\alpha \mathbf{u}_\alpha) = \varrho_\alpha F_\alpha, \quad (1)$$

and the Darcy law for the phase α reads as

$$\mathbf{u}_\alpha = -\frac{k_{r,\alpha}}{\mu_\alpha} \mathbf{K}(\nabla p_\alpha - \varrho_\alpha \mathbf{g}) = -\lambda_\alpha \mathbf{K}(\nabla p_\alpha - \varrho_\alpha \mathbf{g}), \quad (2)$$

where ϕ [–] is the porosity of the medium, \mathbf{K} [m^2] is the intrinsic permeability tensor, and \mathbf{g} [$m s^{-2}$] is the gravitational acceleration vector. For $\alpha \in \{w, n\}$, the symbols ϱ_α , S_α , \mathbf{u}_α , F_α , μ_α , $k_{r,\alpha}$, and p_α stand for the α -phase density [$kg m^{-3}$], saturation [–], apparent macroscopic velocity [$m s^{-1}$], specific source/sink term [s^{-1}], dynamic viscosity [$kg m^{-1} s^{-1}$], relative permeability [–], and pressure [$kg m^{-1} s^{-2}$], respectively. The term $k_{r,\alpha}/\mu_\alpha$ is frequently denoted as the α -phase mobility λ_α . By definition, $S_w + S_n = 1$. We use the *Burdine* model for the relative permeability functions

$$k_{r,w}(S_{w,e}) = S_{w,e}^{3+\frac{2}{\lambda}}, \quad k_{r,n}(S_{w,e}) = (1 - S_{w,e})^2(1 - S_{w,e}^{1+\frac{2}{\lambda}}), \quad (3)$$

where the parameter λ [–] is determined experimentally and $S_{w,e}$ is the effective wetting-phase saturation defined as $S_{w,e} = (S_w - S_{wr})/(1 - S_{wr})$, where S_{wr} is the irreducible wetting-phase saturation.

The effects of capillarity are modeled by the capillary pressure $p_c = p_n - p_w$ which is considered to be a function of saturation S_w . A commonly acknowledged model for drainage processes for $p_c = p_c(S_w)$ is the Brooks and Corey model

$$p_c(S_{w,e}) = p_d S_{w,e}^{-\frac{1}{\lambda}} \quad \text{for } S_{w,e} \in (0, 1], \quad (4)$$

where λ is the same parameter as in (3) and p_d [Pa] is the *entry pressure*. The entry pressure p_d is the capillary pressure at full saturation and it is the minimal capillary pressure required to displace the wetting phase from the largest occurring pore. It plays an important role in the flow of non-wetting phases through material interfaces. Let us consider an initially fully water saturated column with two sands separated by a sharp interface. Since no mass is lost or produced at the material interface, the mass conservation law states that the normal component of the *mass flux* $Q_\alpha \mathbf{u}_\alpha \cdot \mathbf{n}$ is continuous across the interface, where \mathbf{n} denotes a unit normal to the interface (see Figure 1). Assuming that a mobile wetting phase is present on both sides of the interface, it follows that p_w is also continuous across the interface (c.f. [9]). Moreover, if a non-wetting phase is present on both sides of the interface, p_n is also assumed to be continuous which implies the continuity of the capillary pressure p_c in that case. On the other hand, if the non-wetting phase is not present but approaches the material interface from the coarse sand side (denoted by the superscript I), the interfacial capillary pressure p_c^I increases. When p_c^I is lower than p_d^{II} of the finer medium, the non-wetting phase cannot penetrate the interface and accumulates there. In this case both p_c and p_n are discontinuous. This is referred to as the *barrier effect* [9]. Once the capillary pressure p_c^I exceeds the entry pressure threshold p_d^{II} , the non-wetting phase enters the finer medium and the capillary pressure p_c is continuous, i.e., $p_c^I = p_c^{II}$, while the saturation can be still discontinuous. In Figure 2, typical Brooks and Corey capillary pressure curves (4) for two different porous media are shown. Altogether, the condition at the material interface is established in the following form:

$$\begin{aligned} S_n^{II} = 0 \quad \text{and} \quad p_c^{II} = p_d^{II}, \quad \text{if} \quad p_c^I < p_d^{II}, \\ p_c^I = p_c^{II}, \quad \text{otherwise.} \end{aligned} \tag{5}$$

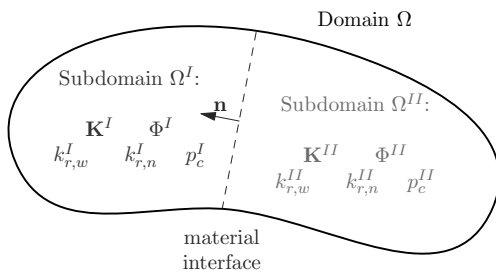


Figure 1: The sharp interface between two different porous media.

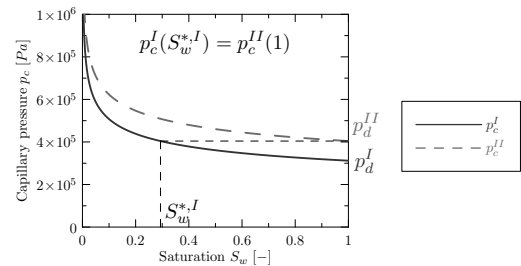


Figure 2: Typical Brooks and Corey p_c curves for two different sands.

Eq. (5) is referred to as the *extended capillary pressure condition* [9]. A unique value of the wetting phase saturation $S_w^{I,*}$ can be associated with the threshold value of the capillary pressure such that $S_w^{I,*} = (p_c^I)^{-1}(p_d^{II})$, see Figure 2. The threshold saturation $S_w^{I,*}$ indicates whether the non-wetting phase can penetrate the material interface ($S_w^I \leq S_w^{I,*}$) or the barrier effect is simulated ($S_w^I > S_w^{I,*}$).

3. Problem Formulation

We assume that both fluids are incompressible, we introduce the *flow potential* ψ_α as $\psi_\alpha = p_\alpha - Q_\alpha \mathbf{g} \cdot \mathbf{x}$, where \mathbf{x} is the position vector and $\alpha \in \{w, n\}$. Similarly to the definition of the capillary pressure, we define the *capillary potential* as

$$\psi_c = \psi_n - \psi_w = p_c - (\rho_n - \rho_w)\mathbf{g} \cdot \mathbf{x}. \tag{6}$$

Consequently, the system of equations can be rewritten in the following form

$$\phi \frac{\partial S_\alpha}{\partial t} + \nabla \cdot \mathbf{u}_\alpha = F_\alpha, \tag{7a}$$

$$\mathbf{u}_\alpha = -\lambda_\alpha \mathbf{K} \nabla \psi_\alpha, \tag{7b}$$

$$\psi_c = \psi_n - \psi_w, \tag{7c}$$

$$S_w + S_n = 1, \tag{7d}$$

where $\alpha \in \{w, n\}$ and the unknown functions are the saturations $S_\alpha = S_\alpha(t, \mathbf{x})$ and the phase potentials $\psi_\alpha = \psi_\alpha(t, \mathbf{x})$ for all $t > 0$ and \mathbf{x} inside a domain $\Omega \subset \mathbb{R}^d$, $d = 1, 2, 3$. Equations (7) are subject to an initial condition

$$S_\alpha = S_\alpha^{ini}, \quad \text{in } \Omega, \tag{8}$$

and boundary conditions

$$\mathbf{u}_\alpha \cdot \mathbf{n} = u_\alpha^N \quad \text{on } \Gamma_{\mathbf{u}_\alpha} \subset \partial\Omega, \tag{9a}$$

$$S_w = S_w^D \quad \text{on } \Gamma_{S_w} \subset \partial\Omega, \tag{9b}$$

$$\psi_\alpha = \psi_\alpha^D \quad \text{on } \Gamma_{\psi_\alpha} \subset \partial\Omega, \tag{9c}$$

where $\Gamma_{\mathbf{u}_\alpha}$, Γ_{S_w} , and Γ_{ψ_α} denote the subsets of the domain boundary $\partial\Omega$ where the boundary conditions for \mathbf{u}_α , S_w , and ψ_α are prescribed, respectively, $\alpha \in \{w, n\}$. The initial condition (8) and boundary conditions (9) should be consistent with (7c) and (7d).

Summing (7a) over $\alpha = \{w, n\}$ and using (7d), we obtain the following equation for the divergence of the *total velocity* $\mathbf{u}_t = \mathbf{u}_w + \mathbf{u}_n$,

$$\nabla \cdot \mathbf{u}_t = \nabla \cdot (\mathbf{u}_w + \mathbf{u}_n) = F_w + F_n \quad \text{in } \Omega. \tag{10}$$

We define new velocities \mathbf{u}_a and \mathbf{u}_c

$$\mathbf{u}_a = -\lambda_t \mathbf{K} \nabla \psi_w, \quad \mathbf{u}_c = -\lambda_t \mathbf{K} \nabla \psi_c, \tag{11}$$

where the velocity \mathbf{u}_a has the same driving force as the velocity \mathbf{u}_w but with a smoother total mobility $\lambda_t = \lambda_w + \lambda_n$ and the velocity \mathbf{u}_c includes the capillary driving forces. Hence, the total velocity \mathbf{u}_t reads as $\mathbf{u}_t = \mathbf{u}_a + f_n \mathbf{u}_c$, where $f_n = \lambda_n / \lambda_t$ is the fractional flow function of the non-wetting phase. Note that definition (11) is different from the definition of $\mathbf{u}_c^{HF} = -\lambda_n \mathbf{K} \nabla \psi_c$, in [8]. In (11) the term $\lambda_t \mathbf{K}$ is invertible unlike the term $\lambda_n \mathbf{K}$ in \mathbf{u}_c^{HF} which may degenerate.

Consequently, the phase velocities \mathbf{u}_w and \mathbf{u}_n , can be expressed in terms of \mathbf{u}_a and \mathbf{u}_c as

$$\mathbf{u}_w = f_w \mathbf{u}_a, \quad \mathbf{u}_n = f_n \mathbf{u}_a + f_n \mathbf{u}_c, \tag{12}$$

where $f_w = \lambda_w / \lambda_t$ is the fractional flow function of the wetting phase. The evolution equation for the wetting phase saturation (7a) in terms of \mathbf{u}_a reads as

$$\phi \frac{\partial S_w}{\partial t} + \nabla \cdot (f_w \mathbf{u}_a) = F_w. \tag{13}$$

4. Discretization

We consider a spatial discretization \mathcal{K}_h of the polygonal domain Ω consisting of elements K , where K are segments in \mathbb{R} or triangles in \mathbb{R}^2 and $h > 0$ is the *mesh size* defined as the maximum element diameter. We assume that the mesh is regular and conforming. We denote by \mathcal{V}_h the set of all vertices V of \mathcal{K}_h , by \mathcal{E}_h the set of all sides of \mathcal{K}_h , and by \mathcal{E}_h^{int} and \mathcal{E}_h^{ext} the set of interior and exterior sides of \mathcal{K}_h , respectively. By \mathcal{E}_K , we denote the set of all sides of an element $K \in \mathcal{K}_h$.

4.1. Velocity Approximation

We assume, that the velocities \mathbf{u}_α , where $\alpha \in \{w, n\}$, belong to the functional space $\mathbf{H}(\text{div}, \Omega)$. On each element $K \in \mathcal{K}_h$, we shall approximate the phase velocities \mathbf{u}_α in the lowest order Raviart–Thomas space $\mathbf{RT}_0(K) \subset \mathbf{H}(\text{div}, K)$. The basis functions $\mathbf{w}_{K,E} \in \mathbf{RT}_0(K)$ are chosen such that $\forall E, F \in \mathcal{E}_K$

$$\mathbf{w}_{K,E} \cdot \mathbf{n}_{K,F} = \delta_{EF} \frac{1}{|E|_{d-1}}, \quad \nabla \cdot \mathbf{w}_{K,E} = \frac{1}{|K|_d}, \tag{14}$$

where $\mathbf{n}_{K,E}$ is the outward unit normal to side $E \in \mathcal{E}_K$ with respect to element K , d denotes the space dimension, δ_{EF} is the Kronecker symbol, and $|\cdot|_d$ is a d -dimensional Lebesgue measure. For convenience, we set $|E|_0 = 1$ for all $E \in \mathcal{E}_K$. Assuming that the velocity \mathbf{u}_α is approximated in the basis of $\mathbf{RT}_0(K)$ as

$$\mathbf{u}_\alpha = \sum_{E \in \mathcal{E}_K} u_{\alpha,K,E} \mathbf{w}_{K,E}, \quad \alpha \in \{a, c\}, \tag{15}$$

where $u_{\alpha,K,E}$ are the side-flux variables across the side $E \in \mathcal{E}_K$ in the outward direction with respect to K .

By inverting the permeability tensor \mathbf{K} and the total mobility λ_t in (11), we obtain

$$\lambda_t^{-1} \mathbf{K}^{-1} \mathbf{u}_a = -\nabla \psi_w, \tag{16}$$

where \mathbf{K} is positive definite tensor and λ_t is strictly positive. The variational formulation is obtained by multiplying (16) by the test functions from $\mathbf{RT}_0(\mathcal{K}_h)$ that are represented on each element $K \in \mathcal{K}_h$ by the $\mathbf{RT}_0(K)$ basis functions $\mathbf{w}_{K,E}$. We integrate the resulting product by parts over K and using the properties of the $\mathbf{RT}_0(K)$ basis functions (14) we obtain from the left-hand-side of (16):

$$\int_K \lambda_t^{-1} \mathbf{w}_{K,E} \mathbf{K}^{-1} \mathbf{u}_a = \lambda_{t,K}^{-1} \sum_{F \in \mathcal{E}_K} u_{a,K,F} A_{K,E,F}, \quad \text{where } A_{K,E,F} = \int_K \mathbf{w}_{K,E} \mathbf{K}^{-1} \mathbf{w}_{K,F}, \tag{17}$$

and from the right-hand-side of (16):

$$-\int_K \nabla \psi_w \cdot \mathbf{w}_{K,E} = -\int_{\partial K} \psi_w \mathbf{w}_{K,E} \cdot \mathbf{n}_{\partial K} + \int_K \psi_w \nabla \cdot \mathbf{w}_{K,E} = \frac{1}{|K|_d} \int_K \psi_w - \frac{1}{|E|_{d-1}} \int_E \psi_w = \psi_{w,K} - \psi_{w,E}, \tag{18}$$

where $\lambda_{t,K}$ is the average of λ_t over K and by $\psi_{w,K}$ and $\psi_{w,F}$ we denote the cell- and side-averages of the potential ψ_w , respectively. The coefficients $\{A_{K,E,F}\}_{E,F \in \mathcal{E}_K}$ in (17) form a symmetric and positive definite matrix \mathbf{A}_K on K [8]. Therefore, \mathbf{A}_K is invertible and by $\mathbf{a}_K = \{a_{K,E,F}\}_{E,F \in \mathcal{E}_K}$, we denote its inversion. The coefficients $a_{K,E,F}$ depend only on the mesh \mathcal{K}_h and the value of the intrinsic permeability tensor \mathbf{K} . Using this notation, the side-fluxes $u_{a,K,E}$ satisfy

$$u_{a,K,E} = \lambda_{t,K} \left(a_{K,E} \psi_{w,K} - \sum_{F \in \mathcal{E}_K} a_{K,E,F} \psi_{w,F} \right), \tag{19}$$

where $a_{K,E} = \sum_{F \in \mathcal{E}_K} a_{K,E,F}$. In (19) we assume that the side-average potentials $\psi_{w,E}$ are continuous across the internal sides, i.e., $\psi_{w,K_1,E} = \psi_{w,K_2,E} = \psi_{w,E}$, for all neighboring elements K_1 and K_2 of $E \in \mathcal{E}_h^{int}$. Additionally, we drop out the element index K from the side-average potential $\psi_{w,K,E} = \psi_{w,E}$ also for all external (boundary) sides $E \in \mathcal{E}_h^{ext}$.

Similarly, by virtue of the definition of \mathbf{u}_c in (11), the expression of \mathbf{u}_c in $\mathbf{RT}_0(K)$ reads as

$$u_{c,K,E} = \lambda_{t,K} \left(a_{K,E} \psi_{c,K} - \sum_{F \in \mathcal{E}_K} a_{K,E,F} \psi_{c,K,F} \right), \tag{20}$$

where $\psi_{c,K,F}$ denotes the potential ψ_c averaged over side F with respect to element K for all $F \in \mathcal{E}_K$. Due to the extended capillary pressure condition at a material interface placed at side $E \in \mathcal{E}_h^{int}$, the side-average capillary potential $\psi_{c,E}$ can be discontinuous when the barrier effect is simulated. This situation requires careful treatment and is described in the following section. We drop out the element index K from the side-average potential $\psi_{c,K,E} = \psi_{c,E}$ also for all external (boundary) sides $E \in \mathcal{E}_h^{ext}$.

4.2. System of Equations for Capillary Potentials

Let us consider two neighboring elements K_1 and K_2 . Assuming that no mass is produced or lost on an internal side $E \in \mathcal{E}_{K_1} \cap \mathcal{E}_{K_2}$, we consider the following balance of the normal components of \mathbf{u}_a and \mathbf{u}_c across E (c.f. [8]):

$$u_{\alpha,K_1,E} + u_{\alpha,K_2,E} = 0, \quad \alpha \in \{a, c\}. \tag{21}$$

In order to establish a system of linear equations in terms of the side-average potentials $\psi_{c,K,E}$ for all $E \in \mathcal{E}_h^{int}$, $E \in \mathcal{E}_{K_1} \cap \mathcal{E}_{K_2}$, we combine (20) with (21):

$$\lambda_{t,K_1} a_{K_1,E} \psi_{c,K_1} - \lambda_{t,K_1} \sum_{F \in \mathcal{E}_{K_1}} a_{K_1,E,F} \psi_{c,K_1,F} + \lambda_{t,K_2} a_{K_2,E} \psi_{c,K_2} - \lambda_{t,K_2} \sum_{F \in \mathcal{E}_{K_2}} a_{K_2,E,F} \psi_{c,K_2,F} = 0. \tag{22}$$

If the capillary potential is continuous across side $F \in \mathcal{E}_{K_1} \cap \mathcal{E}_{K_2}$, the side-average potentials $\psi_{c,K_1,F}$ and $\psi_{c,K_2,F}$ coincide and we denote their common value as $\psi_{c,F}$. In case of the barrier effect at side F , the capillary potential is discontinuous across F and by $\psi_{c,F}$ we denote the side-average capillary pressure potential that corresponds to the element with lower entry pressure. Altogether, the following side-average potentials $\psi_{c,K_1,E}$ and $\psi_{c,K_2,E}$ are used in the expression for the side-velocities in (22):

$$\psi_{c,K_1,E} = \begin{cases} p_{d,K_1} - (\rho_n - \rho_w) \int_E \mathbf{g} \cdot \mathbf{x} \, dx, & \text{if } p_{c,K_2,E} < p_{d,K_1}, \\ \psi_{c,E}, & \text{otherwise,} \end{cases} \tag{23a}$$

$$\psi_{c,K_2,E} = \begin{cases} p_{d,K_2} - (\rho_n - \rho_w) \int_E \mathbf{g} \cdot \mathbf{x} \, dx, & \text{if } p_{c,K_1,E} < p_{d,K_2}, \\ \psi_{c,E}, & \text{otherwise.} \end{cases} \tag{23b}$$

In (22), the cell-average capillary potential $\psi_{c,K}$ can be directly computed using (6) for a given cell-average value of the saturation $S_{w,K}$.

Together with the boundary conditions used to close the system of equations (23) for the unknown side-average potentials $\psi_{c,K,E}$, we obtain a system of linear equations that can be written in a matrix form as

$$\mathbf{M}_c \Psi_c = \mathbf{b}_c, \tag{24}$$

where the square, sparse, symmetric, and positive definite matrix \mathbf{M}_c and the vectors Ψ_c and \mathbf{b}_c have dimensions $\#\mathcal{E}_h$, where $\#\mathcal{E}_h$ denotes the total number of sides in \mathcal{E}_h . The components of the vector Ψ_c are the side average potentials $\psi_{c,E}$ for all $E \in \mathcal{E}_h$.

4.3. System of Equations for Wetting-Phase Potentials

In order to express $u_{a,K,E}$ given by (19) in terms of the side-average variables $\psi_{w,E}$ and $\psi_{c,E}$, we derive an explicit formula for the cell-average of the wetting phase potential $\psi_{w,K}$. We integrate the volumetric balance equation (10) for the total velocity \mathbf{u} , over $K \in \mathcal{K}_h$ and use the divergence theorem and the expressions of \mathbf{u}_a and \mathbf{u}_c in $\mathbf{RT}_0(K)$ to obtain

$$\sum_{F \in \partial K} \int_F (\mathbf{u}_a + f_n \mathbf{u}_c) \cdot \mathbf{n}_{K,F} = \sum_{E \in \mathcal{E}_K} u_{a,K,E} + \sum_{E \in \mathcal{E}_K} f_{n,E}^{upw} u_{c,K,E} = F_K, \tag{25}$$

where F_K is the integrated right-hand-side of (10) over K and $f_{n,E}^{upw}$ is the side-average value of f_n taken in the upstream direction with respect to $u_{c,K,E}$. Replacing the side fluxes $u_{a,K,E}$ in (25) by (19), we obtain

$$\psi_{w,K} = \frac{F_K}{\lambda_{t,K} a_K} + \sum_{E \in \mathcal{E}_K} \frac{a_{K,E}}{a_K} \psi_{w,E} - \sum_{E \in \mathcal{E}_K} \frac{f_{n,E}^{upw}}{\lambda_{t,K} a_K} u_{c,K,E}, \tag{26}$$

where $a_K = \sum_{E \in \mathcal{E}_K} a_{K,E}$. Equation (26) allows to express the side fluxes $u_{a,K,E}$ given by (19) in terms of the unknown $\psi_{w,F}$ only

$$u_{a,K,E} = \frac{a_{K,E}}{a_K} \left(F_K - \sum_{F \in \mathcal{E}_K} f_{n,F}^{upw} u_{c,K,F} \right) + \lambda_{t,K} \sum_{F \in \mathcal{E}_K} \left(\frac{a_{K,E} a_{K,F}}{a_K} - a_{K,E,F} \right) \psi_{w,F}. \tag{27}$$

We use (27) in order to express (21) in terms of the side-average potentials $\psi_{w,F}$ and together with the boundary conditions, we obtain a system of linear equations for the unknowns $\psi_{w,F}$ that can be written in the matrix form as

$$\mathbf{M}_a \Psi_w = \mathbf{b}_a, \tag{28}$$

where the square matrix \mathbf{M}_a and the vectors Ψ_w and \mathbf{b}_a have dimensions $\#\mathcal{E}_h$. Similar to the matrix \mathbf{M}_c , the matrix \mathbf{M}_a is sparse, symmetric, and positive definite.

4.4. Saturation Approximation

We discretize the saturation equation (13) using the discontinuous Galerkin (DG) method which is locally conservative and flexible for complex unstructured geometries. The DG method approximates the weak solution $S_w(t, \mathbf{x})$ of (13) in a functional space $D_1(\mathcal{K}_h)$ of discontinuous functions that are piecewise linear on $K \in \mathcal{K}_h$. By $\varphi_{K,E}$, we denote the piecewise linear basis functions of $D_1(\mathcal{K}_h)$ associated with the edges for all $K \in \mathcal{K}_h$ and $E \in \mathcal{E}_K$. We choose $\varphi_{K,E}$ such that $1/|E|_{d-1} \int_E \varphi_{K,F} = \delta_{EF}$ for all $K \in \mathcal{K}_h$, $E, F \in \mathcal{E}_K$, and $d = 1, 2$. In order to obtain the variational formulation of the continuity equation on each element K , we multiply (13) by the basis functions $\varphi_{K,E} \in D_1(\mathcal{K}_h)$, $E \in \mathcal{E}_K$, integrate over K , and using the Green theorem:

$$\int_K \phi \frac{\partial S_w}{\partial t} \varphi_{K,E} + \int_{\partial K} f_w \varphi_{K,E} \mathbf{u}_a \cdot \mathbf{n}_{\partial K} - \int_K f_w \mathbf{u}_a \cdot \nabla \varphi_{K,E} = \int_K F_w \varphi_{K,E}. \tag{29}$$

We express the approximated solution as

$$S_w(t, \mathbf{x}) \approx \sum_{K \in \mathcal{K}_h} \sum_{E \in \mathcal{E}_K} S_{w,K,E}(t) \varphi_{K,E}(\mathbf{x}), \tag{30}$$

for all $\mathbf{x} \in \Omega$ and $t \in (0, T)$, where the basis coefficients $S_{w,K,E}$ are time-dependent. Using the expression of \mathbf{u}_a in the basis of $\mathbf{RT}_0(K)$ in (15), we approximate (29) as

$$\phi_K \sum_{F \in \mathcal{E}_K} \frac{dS_{w,K,F}}{dt} \int_K \varphi_{K,E} \varphi_{K,F} + \sum_{H, F \in \mathcal{E}_K} f_{w,F}^{upw} \frac{u_{a,K,G}}{|H|_{d-1}} \int_H \varphi_{K,F} \varphi_{K,E} - f_{w,K} \sum_{G \in \mathcal{E}_K} u_{a,K,G} \left(\delta_{EG} - \frac{1}{d+1} \right) = \int_K F_w \varphi_{K,E}, \tag{31}$$

where $f_{w,K}$ is the cell-average of f_w , $f_{w,F}^{upw}$ is the side-average of f_w taken in the upstream direction with respect to $u_{a,K,F}$. We use the explicit forward Euler method to solve the system of ODEs (31) where the initial condition is given by the initial condition for the saturation (8). Due to the higher-order approximation of the saturation in the discontinuous Galerkin method, the numerical scheme produces non-physical oscillations near shocks, [10], [8]. These spurious oscillations can be avoided by reconstructing the approximated discontinuous Galerkin solution using a slope limiter procedure. To stabilize the MHFE-DG numerical scheme, we use the slope limiter introduced by Chavent and Jaffré, [11], in the form described in [10].

4.5. Computational Algorithm

We summarize the complete computational algorithm for obtaining the numerical solution of the two-phase flow system (7) using the MHFE-DG method. The computation proceeds in the following order:

1. Compute the mesh-dependent coefficients $a_{K,E,F}$, $a_{K,E}$, and a_K for all $K \in \mathcal{K}_h$ and $E, F \in \mathcal{E}_K$.
2. Set $i = 0$, $t = t_0$, and choose an initial time step Δt_0 . Use (8) to initialize $S_{w,K,E}^0 = S_{w,K,E}^{ini}$.
3. Repeat the following steps until the predetermined final time T of the simulation is reached.
 - (a) Based on a given saturations $S_{w,K,E}^i$ from previous time t_i , compute the cell-average capillary potentials $\psi_{c,K}$ for all $K \in \mathcal{K}_h$ using (6).
 - (b) Assemble \mathbf{M}_c and \mathbf{b}_c , solve (24), and compute $u_{c,K,E}$ for all $K \in \mathcal{K}_h$ and $E \in \mathcal{E}_K$ using (20).
 - (c) Assemble \mathbf{M}_a and \mathbf{b}_a , solve (28), and compute $u_{a,K,E}$ for all $K \in \mathcal{K}_h$ and $E \in \mathcal{E}_K$ using (27).
 - (d) Use the forward Euler method to obtain $S_{w,K,E}^{i+1}$ from (31).
 - (e) Apply the slope limiting procedure in the form described in [10].
 - (f) Set $t_{i+1} = t_i + \Delta t_i$ and set $i := i + 1$.

5. Numerical Experiments

The correctness and accuracy of the MHFE-DG numerical scheme is verified by means of the semi-analytical solutions that can be obtained if several assumptions are placed upon the problem formulation (7). These benchmark solutions can be derived for a one-dimensional two-phase flow problem without sources or sinks ($F_w = F_n = 0$) and

$h_1 \rightarrow h_2$ [cm]	Homogeneous Case		Heterogeneous Case	
	eoc_1	eoc_2	eoc_1	eoc_2
$1 \rightarrow 1/2$	0.91	0.75	0.87	0.62
$1/2 \rightarrow 1/4$	0.92	0.89	0.93	0.72
$1/4 \rightarrow 1/8$	0.83	1.041	0.91	0.63
$1/8 \rightarrow 1/16$	0.53	1.32	0.92	0.63

Table 1: Experimental orders of convergence eoc_1 and eoc_2 computed for the benchmark problems in homogeneous (left column) and heterogeneous (right column) porous medium in L_1 and L_2 norms, respectively.

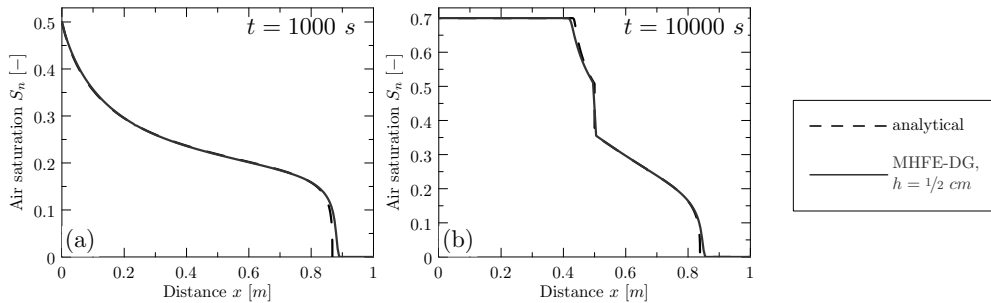


Figure 3: Numerical solution of the McWhorter and Sunada problem in a homogeneous (a) and heterogeneous (b) porous medium.

with zero gravity ($\mathbf{g} = 0$) for homogeneous and heterogeneous cases, see [12], [13], and [14]. In both benchmark problems we assume that the air ($\mu_a = 1.8205 \cdot 10^{-5} \text{ kg m}^{-1} \text{ s}^{-1}$ and $\rho_a = 1.2 \text{ kg m}^{-3}$) displaces water ($\mu_w = 0.001 \text{ kg m}^{-1} \text{ s}^{-1}$ and $\rho_w = 1000 \text{ kg m}^{-3}$) from a one-dimensional domain.

In homogeneous case, we test the numerical scheme by means of the McWhorter and Sunada [15] exact solution in a one-dimensional domain $\Omega = [0, 1]$ with the following choice of the parameters: $R = 0.92$, $S_0 = 0.5$, $S_i = 1$, and $A = 1.53 \cdot 10^{-3} \text{ ms}^{-1/2}$ (for the definition of these parameters, we refer to [13]). The properties of the porous medium are given in Table 2, Sand F. In the MHFE-DG numerical scheme, we set $S_w^{ini} = S_i = 1$ and at $x = 0$, we prescribe the air and water Neumann boundary velocities to $u_n^N(t, 0) = At^{-1/2}$ and $u_w^N(t, 0) = (R - 1)At^{-1/2}$, respectively. At the outlet ($x = 1 \text{ m}$), we set $u_w^N(t, 1) = RA t^{-1/2} \text{ ms}^{-1}$ and $S_w^D(t, 1) = S_i = 1$. We choose the final time $T = 1000 \text{ s}$ so that the air-front stays inside Ω .

In case of heterogeneous porous medium, we consider the Fučík *et al.* semi-analytical solution described in [14] with the following choice of parameters: $R = 0.9$, $S_i^I = 0.3$, and $S_i^H = 1$ (for the definition of these parameters, we refer to [14]). The properties of the Sand F in $\Omega^I = [0, 1/2]$ and Sand G in $\Omega^H = [1/2, 1]$ are given in Table 2. In the numerical model, we use the following initial and boundary conditions. Initially, $S_w(0, x) = 0.3$ in Ω^I and $S_w(0, x) = 1$ in Ω^H . At $x = 0$, we set $S_w^D(t, 0) = 0.3$ and $\psi^D(t, 0) = 0 \text{ Pa}$. The boundary conditions at $x = 1$ read as $u_n^N(t, 1) = 0 \text{ ms}^{-1}$ and $u_w^N(t, 1) = RA t^{-1/2}$, where $A = 5.61 \cdot 10^{-4} \text{ ms}^{-1/2}$.

We compute the numerical solutions on a series of regular meshes with decreasing mesh sizes and constant ratio $\Delta t/h^2$ and compare them to the semi-analytical solution in Figure 3. We present the experimental orders of convergence (eoc) in Table 1 and show that the MHFE-DG method converge towards the exact solution.

6. Simulation of Laboratory Experiment

As an example of applicability of the MHFE-DG method, we choose to simulate the random medium laboratory experiment described in [16], [17], and [3]. We model immiscible and incompressible injection of a light NAPL (LNAPL) with ($\mu_n = 0.0035 \text{ kg m}^{-1} \text{ s}^{-1}$ and $\rho_n = 830 \text{ kg m}^{-3}$) into an initially fully water saturated two dimensional domain. The domain consists of a stochastically generated heterogeneous layer that is inclined between two homogeneous ones, see Figure 4b. Properties of sands are given in Table 2. Throughout the domain, a slow flow from right to left is imposed by an increased water head at the right-hand-side boundary. At $t = 0$, LNAPL starts to be injected into

the source zone (see Figure 4b) with a constant rate of 53 mg s^{-1} up to $t = 9490 \text{ s}$. Then, the influx was stopped. Since our improved MHFE-DG approach is designed to capture sharp material interfaces between neighboring elements, we use the mesh shown in Figure 4a that exactly coincides with the random distribution of the heterogeneous sand blocks. In Figure 5, we plot the LNAPL saturation distribution at $t = 0.5h, 2h, 4h$, and $5h$. The LNAPL patterns are in a good agreement with the laboratory measured non-wetting phase saturation patterns presented in [16], [17], and [3].

7. Conclusion

We used the mixed-hybrid finite element (MHFE) method together with the discontinuous Galerkin (DG) approach to develop a modern numerical scheme capable of simulating flow of two immiscible and incompressible fluids in heterogeneous porous materials. We extended the approach described in [8] so that the barrier pooling at material interfaces can be simulated. We used the previously developed benchmark solutions to investigate the convergence of the MHFE-DG numerical scheme towards the exact solution in both homogeneous and layered materials. In order to demonstrate applicability of the MHFE-DG method in a highly heterogeneous medium, we simulated a laboratory experiment described in [16], [17], and [3]. The numerical approximation of the NAPL distribution shows remarkably good correspondance to the laboratory measured NAPL saturations in [17] indicating that the barrier effect is simulated correctly.

Acknowledgment

The authors would like to thank Tissa H. Illangasekare, Colorado School of Mines, Golden, CO and Fritjof Fagerlund, Uppsala University, Sweden for providing experimental data. Partial support of the project "Development of computer models of CO_2 sequestration in the subsurface" P105/11/1507 of the Czech Science Foundation and the project "Numerical Methods for Multiphase Flow and Transport in Subsurface Environmental Applications" KON-TAKT ME10009, Czech Ministry of Education, Youth and Sports is acknowledged.

Property		Sand A	Sand B	Sand C	Sand D	Sand E	Sand F	Sand G
Entry pressure	p_d [Pa]	363	484	1051	1380	2419	3450	4042
Porosity	ϕ [-]	0.43	0.40	0.43	0.40	0.44	0.448	0.418
Int. permeability	K [10^{-11}m^2]	170	61	18	6.6	2.2	1.631	1.437
Residual saturation	S_{wr} [-]	0.11	0.06	0.06	0.11	0.06	0.265	0.037
Pore size dist. index	λ [-]	4.8	2.77	3.28	3.04	2.70	4.660	5.323

Table 2: Properties of sands used in the numerical simulation (taken over from [3]).

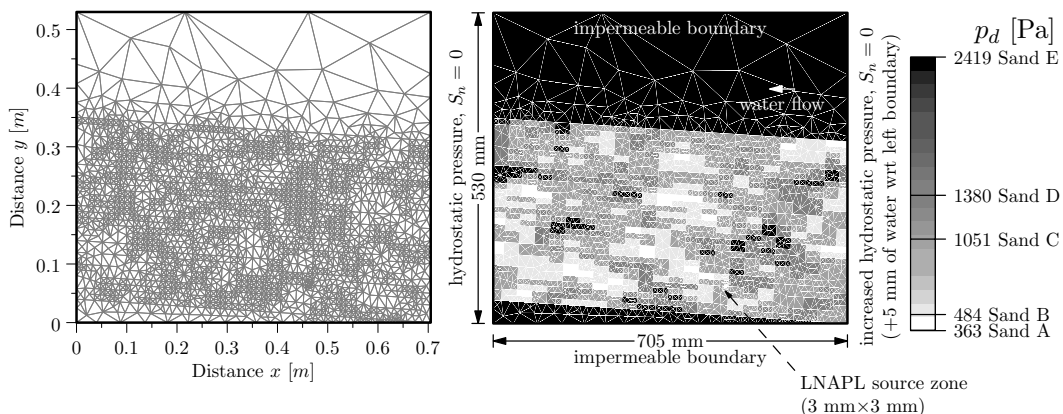


Figure 4: Sand distribution and boundary conditions for the random heterogeneous medium simulation.

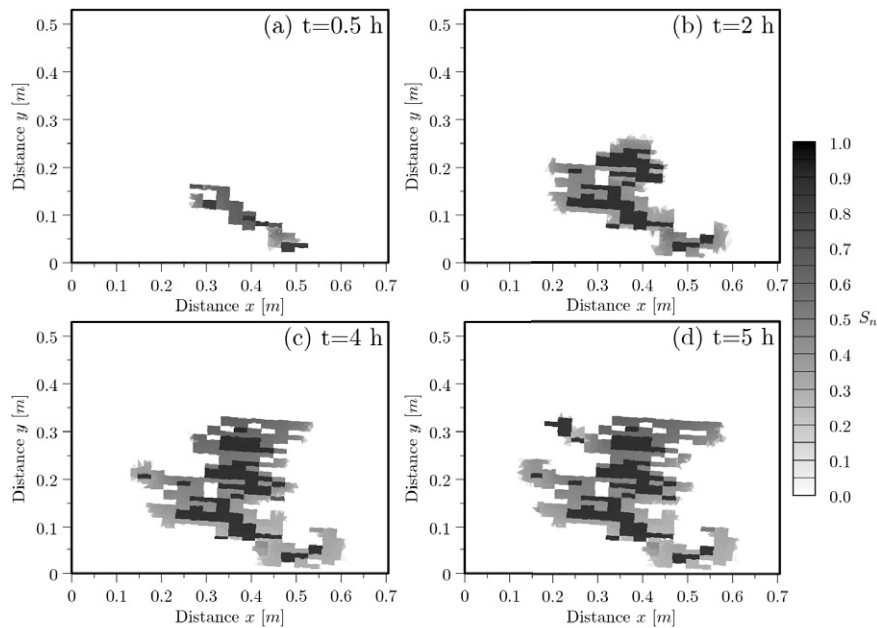


Figure 5: Simulated LNAPL saturation S_n in the random heterogeneous medium computed using the MHFE-DG numerical scheme. The time step Δt is chosen adaptively.

References

- [1] J. Bear, A. Verruijt, Modeling Groundwater Flow and Pollution, D. Reidel, Holland, Dordrecht, 1990.
- [2] R. Helmig, Multiphase Flow and Transport Processes in the Subsurface: A Contribution to the Modeling of Hydrosystems, Springer Verlag, Berlin, 1997.
- [3] J. Mikyška, M. Beneš, T. H. Illangasekare, Numerical Investigation of Non-Aqueous Phase Liquid Behavior at Heterogeneous Sand Layers Using VODA Multiphase Flow Code, *Journal of Porous Media* 12 (7) (2009) 685–694.
- [4] J. Mikyška, A. Firoozabadi, Implementation of Higher-Order Methods for Robust and Efficient Compositional Simulation, *Journal of Computational Physics* (229) (2010) 2898–2913.
- [5] D. Nayagam, G. Schäfer, R. Mosé, Modelling Two-Phase Incompressible Flow in Porous Media Using Mixed Hybrid and Discontinuous Finite Elements, *Computational Geosciences* 8 (1) (2004) 49–73.
- [6] H. Hoteit, A. Firoozabadi, Multicomponent Fluid Flow by Discontinuous Galerkin and Mixed Methods in Unfractured and Fractured Media, *Water Resources Research* 41.
- [7] H. Hoteit, A. Firoozabadi, An Efficient Numerical Model for Incompressible Two-Phase Flow in Fractured Media, *Advances in Water Resources* 31 (6) (2008) 891–905.
- [8] H. Hoteit, A. Firoozabadi, Numerical Modeling of Two-Phase Flow in Heterogeneous Permeable Media with Different Capillarity Pressures, *Advances in Water Resources* 31 (1) (2008) 56–73.
- [9] M. I. de Neef, J. Molenaar, Analysis of DNAPL Infiltration in a Medium with a Low-Permeable Lens, *Computational Geosciences* 1 (1997) 191–214.
- [10] H. Hoteit, P. Ackerer, R. Mosé, J. Erhel, B. Philippe, New Two-Dimensional Slope Limiters for Discontinuous Galerkin Methods on Arbitrary Meshes, *Int. J. Numer. Meth. Engng.* (61) (2004) 2566–2593.
- [11] G. Chavent, J. Jaffré, Mathematical Models and Finite Elements for Reservoir Simulation., North-Holland: Amsterdam, 1986.
- [12] M. Beneš, R. Fučík, J. Mikyška, T. H. Illangasekare, Analytical and Numerical Solution for One-Dimensional Two-Phase Flow in Homogeneous Porous Medium, *Journal of Porous Media* 12 (12) (2009) 1139–1152.
- [13] R. Fučík, J. Mikyška, M. Beneš, T. H. Illangasekare, An Improved Semi-Analytical Solution for Verification of Numerical Models of Two-Phase Flow in Porous Media, *Vadose Zone Journal* 6 (1) (2007) 93–104.
- [14] R. Fučík, J. Mikyška, M. Beneš, T. H. Illangasekare, Semianalytical Solution for Two-Phase Flow in Porous Media with a Discontinuity, *Vadose Zone Journal* 7 (3) (2008) 1001–1007.
- [15] D. B. McWhorter, D. K. Sunada, Exact Integral Solutions for Two-Phase Flow, *Water Resources Research* 26 (3) (1990) 399–413.
- [16] F. Fagerlund, T. H. Illangasekare, A. Niemi, Nonaqueous-Phase Liquid Infiltration and Immobilization in Heterogeneous Media: 2. Application to Stochastically Heterogeneous Formations, *Vadose Zone Journal* 6 (3) (2007) 483.
- [17] F. Fagerlund, A. Niemi, T. H. Illangasekare, Modeling of Nonaqueous Phase Liquid (NAPL) Migration in Heterogeneous Saturated Media: Effects of Hysteresis and Fluid Immobility in Constitutive Relations (DOI 10.1029/2007WR005974), *Water Resources Research* 44 (3) (2008) 3409.